Multiple-relaxation-time lattice Boltzmann scheme for homogeneous mixture flows with external force

Submitted for publication to "Physical Review E", code EP10271, version B

Multiple–relaxation–time Lattice Boltzmann Scheme for Homogeneous Mixture Flows with External Force

Pietro Asinari

Department of Energetics, Politecnico di Torino,

Corso Duca degli Abruzzi 24, Torino, Italy

(Dated: March 31, 2008)

Abstract

A new LBM scheme for homogeneous mixture modeling, based on the multiple–relaxation–time (MRT) formulation, which fully recovers Maxwell–Stefan diffusion model in the continuum limit with (a) external force and (b) tunable Schmidt number, is developed. The proposed MRT formulation is based on the theoretical basis of a recently proposed BGK-type kinetic model for gas mixtures [P. Andries, K. Aoki and B. Perthame, JSP, Vol. 106, N. 5/6, 2002] and it substantially extends the applicability of a scheme already proposed by the same author, which used only one relaxation parameter. The recovered equations at macroscopic level are derived by an innovative expansion technique, based on the Grad moment system. Some numerical simulations are reported for the solvent test case with external force, aiming to find out the numerical ranges for the transport coefficients which ensure acceptable accuracies. The numerical results prove a contraction of the theoretical expectations, which are based on a strong separation among the characteristic scales.

PACS numbers: 47.11.-j, 05.20.Dd

I. INTRODUCTION

Recently, the lattice Boltzmann method (LBM) has been proposed as simple alternative to solve simplified kinetic models. Starting from some pioneer works [1–3], the method has reached a more systematic fashion [4, 5] by means of a better understanding of the connections with the continuous kinetic theory [6, 7] and by widening the set of applications, which can benefit from this numerical technique. Depending on the considered LBM scheme and the particular application, the final goal may be to solve the macroscopic equations recovered in the continuum limit (in this case, LBM works as an alternative macroscopic solver) and/or to catch rarefaction effects (which usually require larger computational stencils and make LBM similar to kinetic discrete–velocity models).

When complex fluids are considered and the inter–particle interactions must be taken into account, the discretized models derived by means of the lattice Boltzmann method may offer some computational advantages over continuum based models, particularly for large parallel computing. In order to appreciate the connection between the lattice Boltzmann method and the conventional finite–difference techniques, it is useful to recognize that this method can be considered a sub–class of the fully–Lagrangian methods [8, 9]. A more complete and recent coverage of various previous contributions on LBM is beyond the purposes of the present paper, but can be found in some review papers [10, 11] and some books [12–14].

In the present paper, the attention will be focused on the development of an LBM scheme for *homogeneous mixture* modeling in the continuum limit. A lot of work has been performed in recent years in order to produce reliable lattice Boltzmann models for this application. See Ref. [15] and the bibliography therein for a complete discussion of this topic.

Among the most meaningful, an LBM scheme [16], which is very close to the Hamel model approach [17, 18], has been recently proposed by means of a variational procedure aiming to minimize a proper H function defined on the discrete lattice [16]. In particular, this scheme [16] has the advantage to highlight that, when more than two components are considered, the macroscopic equations, recovered by the model in the continuum limit and ruling the mass transfer, should approach the macroscopic Maxwell–Stefan model, which properly takes into account non-ideal effects (osmotic diffusion, reverse diffusion and diffusion barrier), neglected by simpler Fick model. (a) Unfortunately this model consistently recovers the Maxwell–Stefan diffusion equations in the continuum limit only within the

macroscopic mixture-averaged approximation [19], i.e. only if proper mixture-averaged diffusion coefficients for each component are considered. (b) Moreover this model, like all the previous ones strictly based on the Hamel model, can not satisfy the Indifferentiability Principle [20] prescribing that, if a BGK-like equation for each component is assumed, this set of equations should reduce to a single BGK-like equation, when mechanically identical components are considered.

In order to fix both the previous problems, a new LBM scheme has been proposed [15]. As a theoretical basis for the development of the LBM scheme, a BGK-type kinetic model for gas mixtures, recently proposed by Andries, Aoki and Perthame [21], was considered (in the following referred as the AAP model). The main idea of the new LBM scheme is very simple: the Maxwell–Stefan model can be obtained in LBM models by allowing momentum exchange among different components according to the Maxwell–Stefan prescriptions. As side effect, the obtained model satisfies the Indifferentiability Principle.

Even though the previous model [15] pointed in the in right direction, it was still effected by the limit of the single–relaxation–time formulation. In particular, this does not allow one to tune the kinematic viscosity independently on the diffusion transport coefficients and consequently to tune the Schmidt number, i.e. the ratio between the kinematic viscosity of the mixture and the diffusion coefficient of the single component. Clearly this reduces the applicability of the model discussed in Ref. [15] to those cases where the average mixture transport is substantially zero, or negligible in comparison with the diffusion phenomena. Unfortunately many applications are characterized by a meaningful global transport, ruled by the total pressure gradients inside the mixture [19].

Hence the goal of this paper is twofold:

- to design a multiple–relaxation–time (MRT) formulation of the already proposed model [15] and to prove that the recovered equations at macroscopic level are consistent with the Maxwell–Stefan model with external force, by means of an innovative expansion technique based on the Grad moment system;

- to discuss the implementation of a generic external force in the numerical scheme, by keeping it as general as possible, but compatible with the assumption of low Mach number flows, as usual prescribed by the lattice Boltzmann schemes.

This paper is organized as follows. In Section II, the proposed multiple–relaxation–time

(MRT) LBM scheme is presented, the macroscopic equations are derived by means of an innovative expansion based on the Grad moment system and finally some details for an efficient implementation are discussed. Section III reports some numerical results for the solvent test with external force: in particular, the numerical ranges for the Schmidt numbers are obtained by discussing the desired accuracies with regards to the diffusion transport coefficients. Finally, Section IV summarizes the main results of the paper.

II. MRT LATTICE BOLTZMANN SCHEME

A. AAP model with forcing

Numerous model equations are influenced by Maxwell's approach to solve the Boltzmann equation by using the properties of the Maxwell particles [22] and the linearized Boltzmann equation. The simplest model equations for a binary mixture is that by Gross and Krook [23], which is an extension of the single-relaxation-time model for a pure system, i.e. the celebrated Bhatnagar-Gross-Krook (BGK) model [24]. A complete review of the BGK-type kinetic models for mixtures can be found in Ref. [21] and, concerning the pseudo-kinetic models for LBM schemes, in Ref. [25].

In this paper, we focus on the BGK-type model proposed by Andries, Aoki and Perthame [21], which will be referred to in the following as AAP model, in case of isothermal flow, which is enough to highlight the main features. A complete derivation and discussion of the LBM scheme based on the AAP model without external forcing and with elementary single-relaxation-time formulation can be found in Ref. [15]. The model shows some interesting theoretical features, in particular in terms of satisfying the Indifferentiability Principle and fully recovering the macroscopic Maxwell–Stefan model equations in the continuum limit [15]. In this paper, (a) the external forcing implementation and (b) a MRT formulation for this model will be developed.

The AAP model is based on only one *global* (i.e., taking into account all the component ς) operator for each component σ, namely

$$\frac{\partial f_\sigma}{\partial \hat{t}} + V_i \frac{\partial f_\sigma}{\partial \hat{x}_i} = A_\sigma \left[f_{\sigma(*)} - f_\sigma \right] + d_\sigma, \tag{1}$$

where $\hat{x}_i$, $\hat{t}$, and V_i are the space coordinate divided by the mean free path, the time divided by the mean collision time and the discrete molecular velocity divided by the average

molecular speed respectively (Boltzmann scaling); (1) $f_{\sigma(*)}$ is the equilibrium distribution function for the component σ; (2) A_σ is the linear collisional operator, which, according to the previous scaling, is made by constants of the order of unit; and finally (3) d_σ is the forcing term.

Since LBM does not need to give the accurate behavior of rarefied gas flows, a simplified kinetic equation, such as the discrete velocity model of isothermal BGK equation with constant collision frequencies is often employed as its theoretical basis. The set of considered discrete velocities is the so-called *lattice*. In particular, V_i is a list of i-th components of the velocities in the considered lattice and $f = f_{\sigma(*)}, f_\sigma$ is a list of discrete distribution functions corresponding to the velocities in the considered lattice. Let us consider the two dimensional 9 velocity model, which is called D2Q9. In D2Q9 model, the molecular velocity V_i has the following 9 values:

$$V_1 = \Big[\ 0 \quad 1 \quad 0 \quad \text{-1} \quad 0 \quad 1 \quad \text{-1} \quad \text{-1} \quad 1 \ \Big]^T, \tag{2}$$

$$V_2 = \Big[\ 0 \quad 0 \quad 1 \quad 0 \quad \text{-1} \quad 1 \quad 1 \quad \text{-1} \quad \text{-1} \ \Big]^T. \tag{3}$$

The components of the molecular velocity V_1 and V_2 are the lists with 9 elements.

In the following subsections, the main elements of the scheme, i.e. (1) the definition of the local equilibrium $f_{\sigma(*)}$, (2) the linear collisional operator A_σ and (3) the forcing term d_σ, will be discussed.

1. Local equilibrium

Before proceeding to the definition of the local equilibrium function $f_{\sigma(*)}$, we define the rule of computation for the list. Let h and g be the lists defined by $h = [h_0, h_1, h_2, \cdots, h_8]^T$ and $g = [g_0, g_1, g_2, \cdots, g_8]^T$. Then, hg is the list defined by $[h_0 g_0, h_1 g_1, h_2 g_2, \cdots, h_8 g_8]^T$. The sum of all the elements of the list h is denoted by $\langle h \rangle$, i.e. $\langle h \rangle = \sum_{i=0}^{8} h_i$. Then, the (dimensionless) density $\hat{\rho}_\sigma$ and momentum $\hat{q}_{\sigma i} = \hat{\rho}_\sigma \hat{u}_{\sigma i}$ are simply defined by

$$\hat{\rho}_\sigma = \langle f_\sigma \rangle, \qquad \hat{q}_{\sigma i} = \langle V_i f_\sigma \rangle. \tag{4}$$

Contrarily to what happens for the single fluid modeling, the previous momentum is not used in the definition of the local equilibrium. The key idea of the AAP model is that the

local equilibrium is expressed as a function of a special velocity $\hat{u}^*_{\sigma i}$, which depends on *all the single component velocities*, namely

$$\hat{u}^*_{\sigma i} = \hat{u}_{\sigma i} + \sum_{\varsigma} \frac{m^2}{m_\sigma m_\varsigma} \frac{B_{\sigma\varsigma}}{B_{m\,m}} \hat{x}_\varsigma (\hat{u}_{\varsigma i} - \hat{u}_{\sigma i}), \tag{5}$$

where m_σ and m_ς are the molecular weights for the component σ and ς respectively; $\hat{x}_\varsigma = \hat{\rho}_\sigma / \hat{\rho}$ (where $\hat{\rho} = \sum_\sigma \hat{\rho}_\sigma$) is the mass concentration; m is the mixture averaged molecular weight defined as $1/m = \sum_\sigma \hat{x}_\sigma / m_\sigma$ or equivalently $m = \sum_\sigma \hat{y}_\sigma m_\sigma$; and finally $B_{\sigma\varsigma} = B(m_\sigma, m_\varsigma)$ and $B_{m\,m} = B(m, m)$ are the so-called Maxwell–Stefan diffusion resistance coefficients. The latter parameters can be interpreted as a macroscopic consequence of the interaction potential between component σ and ς and they can be computed as proper integrals of the generic Maxwellian interaction potential (*kinetic way*) or in such a way to recover the desired macroscopic transport coefficients (*fluid–dynamic way*). In particular the generic resistance coefficient is a function of both the interacting component molecular weights, i.e. $B_{\sigma\varsigma} = B(m_\sigma, m_\varsigma)$, and the equilibrium thermodynamic state, which depends on the total mixture properties only.

Introducing the *mass*-averaged mixture velocity, namely

$$\hat{u}_i = \sum_{\varsigma} \hat{x}_\varsigma \hat{u}_{\varsigma i}, \tag{6}$$

the definition given by Eq. (5) can be recasted as

$$\hat{u}^*_{\sigma i} = \hat{u}_i + \sum_{\varsigma} \left(\frac{m^2}{m_\sigma m_\varsigma} \frac{B_{\sigma\varsigma}}{B_{m\,m}} - 1 \right) \hat{x}_\varsigma (\hat{u}_{\varsigma_i} - \hat{u}_{\sigma_i}). \tag{7}$$

Consequently two properties immediately follow. If $m_\sigma = m$ for any component σ, then (Property 1)

$$\hat{u}^*_{\sigma i} = \hat{u}_i + \sum_{\varsigma} \left(\frac{m^2}{mm} \frac{B_{mm}}{B_{mm}} - 1 \right) \hat{x}_\sigma \hat{x}_\varsigma (\hat{u}_{\varsigma i} - \hat{u}_{\sigma i}) = \hat{u}_i. \tag{8}$$

Multiplying Eq. (5) by $\hat{x}_\sigma$ and summing over all the component yields (Property 2)

$$\sum_{\sigma} x_\sigma \hat{u}^*_{\sigma i} = \hat{u}_i + \sum_{\sigma} \sum_{\varsigma} \left(\frac{m^2}{m_\sigma m_\varsigma} \frac{B_{\sigma\varsigma}}{B_{m\,m}} - 1 \right) \hat{x}_\sigma \hat{x}_\varsigma (\hat{u}_{\varsigma i} - \hat{u}_{\sigma i}) = \hat{u}_i. \tag{9}$$

The second property is general, while the first one is valid only for the applicability contest of the Indifferentiability Principle.

By means of the previous quantities, it is possible to define the local equilibrium for the model, namely

$$f_{\sigma(*)\,i} = \hat{\rho}_\sigma\, w_i \left\{ s_{\sigma i} + 3\,(V_{1\,i}\,\hat{u}^*_{\sigma 1} + V_{2\,i}\,\hat{u}^*_{\sigma 2}) + \frac{9}{2}\,(V_{1\,i}\,\hat{u}^*_{\sigma 1} + V_{2\,i}\,\hat{u}^*_{\sigma 2})^2 - \frac{3}{2}\,[(\hat{u}^*_{\sigma 1})^2 + (\hat{u}^*_{\sigma 2})^2] \right\}, \tag{10}$$

where

$$w = [4/9, 1/9, 1/9, 1/9, 1/9, 1/36, 1/36, 1/36, 1/36]^T\,, \tag{11}$$

while $s_{\sigma 0} = (9 - 5\,\varphi_\sigma)/4$ and $s_{\sigma i} = \varphi_\sigma$ for $1 \leq i \leq 8$. The parameter φ_σ is introduced in order to take into account of different molecular weights m_σ and consequently different internal energies $\hat{e}_\sigma$ for the components, namely $\hat{e}_\sigma = \hat{p}_\sigma/\hat{\rho}_\sigma = \varphi_\sigma/3$. This strategy has been already proved as effective [25] and definitively simpler than other strategies [26]. Clearly $\hat{\rho}_\sigma$ can also be obtained as the moment of $f_{\sigma(*)}$, but this is not the case for $\hat{q}_{\sigma i}$:

$$\hat{\rho}_\sigma = \langle f_{\sigma(*)} \rangle, \qquad \hat{q}^*_{\sigma i} = \langle V_i f_{\sigma(*)} \rangle \neq \hat{q}_{\sigma i} = \langle V_i f_\sigma \rangle. \tag{12}$$

2. Collisional operator

The key idea of the multiple–relaxation–time (MRT) approach [3, 14, 27–29] is to relax differently the discrete moments associated with a given LBM scheme. Even though the total number of linearly independent moments is fixed (equal to the number of lattice nodes Q), the choice of the moments to be considered in the relaxation (collision) process is not unique. This set of moments is usually defined as the "moment basis", because it is possible to compute by them any other high-order moment (clearly in contrast with what happens in continuous kinetic theory). In particular, if the moment basis is selected as orthonormal, then some nice features arise and this may increase the stability issues of the numerical scheme and the efficiency of the computations [28, 29]. In the present paper, a simpler approach will be preferred. For a complete discussion on how to select a proper orthonormal basis for the MRT formulation in case of mixtures see Ref. [25].

Let us define a matrix $M = [1;\, V_1;\, V_2;\, V_1^2;\, V_2^2;\, V_1V_2;\, V_1(V_2)^2;\, (V_1)^2V_2;\, (V_1)^2(V_2)^2]^T$, which

involves proper combinations of the lattice velocity components, namely

$$M = \begin{bmatrix} 1 & 1 & 1 & 1 & 1 & 1 & 1 & 1 & 1 \\ 0 & 1 & 0 & -1 & 0 & 1 & -1 & -1 & 1 \\ 0 & 0 & 1 & 0 & -1 & 1 & 1 & -1 & -1 \\ 0 & 1 & 0 & 1 & 0 & 1 & 1 & 1 & 1 \\ 0 & 0 & 1 & 0 & 1 & 1 & 1 & 1 & 1 \\ 0 & 0 & 0 & 0 & 0 & 1 & -1 & 1 & -1 \\ 0 & 0 & 0 & 0 & 0 & 1 & -1 & -1 & 1 \\ 0 & 0 & 0 & 0 & 0 & 1 & 1 & -1 & -1 \\ 0 & 0 & 0 & 0 & 0 & 1 & 1 & 1 & 1 \end{bmatrix}. \tag{13}$$

Consequently the linear collisional operator A_σ can be defined as $A_\sigma = M^{-1}\Lambda_\sigma M$, where

$$\Lambda_\sigma = \begin{bmatrix} 0 & 0 & 0 & 0 & 0 & 0 & 0 & 0 & 0 \\ 0 & \lambda_\sigma^\delta & 0 & 0 & 0 & 0 & 0 & 0 & 0 \\ 0 & 0 & \lambda_\sigma^\delta & 0 & 0 & 0 & 0 & 0 & 0 \\ 0 & 0 & 0 & \frac{\lambda_\sigma^\xi+\lambda_\sigma^\nu}{2} & \frac{\lambda_\sigma^\xi-\lambda_\sigma^\nu}{2} & 0 & 0 & 0 & 0 \\ 0 & 0 & 0 & \frac{\lambda_\sigma^\xi-\lambda_\sigma^\nu}{2} & \frac{\lambda_\sigma^\xi+\lambda_\sigma^\nu}{2} & 0 & 0 & 0 & 0 \\ 0 & 0 & 0 & 0 & 0 & \lambda_\sigma^\nu & 0 & 0 & 0 \\ 0 & 0 & 0 & 0 & 0 & 0 & 1 & 0 & 0 \\ 0 & 0 & 0 & 0 & 0 & 0 & 0 & 1 & 0 \\ 0 & 0 & 0 & 0 & 0 & 0 & 0 & 0 & 1 \end{bmatrix}. \tag{14}$$

As it will be clarified later on by the asymptotic expansion, λ_σ^δ is the relaxation frequency controlling the diffusion process, while λ_σ^ν and λ_σ^ξ are those controlling the viscous phenomena. Some proper tuning strategy is defined in order to recover the desired transport coefficients in the continuum limit. In particular,

$$\lambda_\sigma^\delta = \lambda_\delta = \frac{\hat{p}\, B_{m\,m}}{\hat{\rho}} = \frac{\hat{p}\, B(m,m)}{\hat{\rho}}, \tag{15}$$

$$\lambda_\sigma^\nu = \lambda_\nu = \frac{1}{3\,\nu}, \tag{16}$$

$$\lambda_\sigma^\xi = \lambda_\xi(2-\varphi_\sigma) = \frac{(2-\varphi_\sigma)}{3\,\xi}, \tag{17}$$

where $\hat{p} = \sum_\sigma \hat{p}_\sigma$, ν is the kinematic viscosity and ξ is a numerical parameter somehow related to the second viscosity coefficient (compressible effects are not rigorously recovered by the considered lattice).

3. Forcing term

The external source d_σ can be directly designed in the moment space as

$$d_\sigma = M^{-1}\left[0,\ \hat{\rho}_\sigma\hat{c}_{\sigma 1},\ \hat{\rho}_\sigma\hat{c}_{\sigma 2},\ \frac{\partial(\hat{\rho}_\sigma\hat{c}_{\sigma 1})}{\partial\hat{x}_1},\ \frac{\partial(\hat{\rho}_\sigma\hat{c}_{\sigma 2})}{\partial\hat{x}_2},\ 0,\ 0,\ 0,\ 0\right]^T, \tag{18}$$

where $\hat{c}_{\sigma i} = \hat{a}_i + \hat{b}_{\sigma i}$ and $\hat{a}_i$ is the acceleration due to an external field acting on all the components in same way (for example, the gravitational acceleration), while $\hat{b}_{\sigma i}$ is the acceleration due to a second external field discriminating the nature of the component particles (for example because of their charge). As it will be clarified later on by the asymptotic expansion, the additional terms affecting the stress tensor components must be considered in order to compensate the deficiencies (in terms of symmetry properties) of the considered lattice. From the computational point of view, if the external force is not homogeneous in space, the previous forcing term must be computed (eventually at each time step) by means of a finite difference formula involving neighboring nodes. This goal can be achieved with second order accuracy on the compact stencil D2Q9.

B. Asymptotic analysis of MRT formulation by Grad moment system

In this section the macroscopic equations of the MRT-LBM scheme are recovered by means of the asymptotic analysis. Many types of asymptotic analysis for LBM exist (Chapman–Enskog expansion, Hilbert expansion, Grad moment expansion,...), which are substantially equivalent for the present purposes. The Chapman–Enskog expansion is still the most popular approach to analyze LBM schemes, even though, concerning mixture modeling, it shows some limits [30]. On the other hand, the Hilbert expansion proposed by Ref. [31] and derived by kinetic theory [32] offers some advantages, even though all the macroscopic moments must be expanded. Recovering macroscopic equations solved by LBM schemes somehow shares some features in common with the much more complex problem of recovering macroscopic equations from kinetic models. A complete review of the latter problem is beyond the purposes of the present paper, but detailed discussions can be found in Refs. [32, 33]. In this paper, we use a simpler approach based on (1) some proper scaling, (2) the Grad moment system and (3) recursive substitutions. The method has been already used in order to derive new numerical schemes [34].

The latter method is not new and it has some features in common with recently proposed asymptotic methods in kinetic theory [35]. Recently the so–called Order of Magnitude Approach has been proposed in order to derive approximations to the Boltzmann equation from its infinite set of corresponding moment equations [33, 36, 37]. This method first determines the order of magnitude of all moments by means of a Chapman–Enskog expansion, forms linear combinations of moments in order to have the minimum number of moments at a given order, and then uses the information on the order of the moments to properly rescale the moment equations. The rescaled moment equations are finally systematically reduced by canceling terms of higher order. Moreover this method can be further simplified.

- Firstly, following Ref. [35], we will directly work on the level of the moment equations. In this way, the key advantage in analyzing LBM schemes in comparison with truly kinetic models is that the moment system is automatically truncated because of the discrete degrees of freedom of the selected lattice and this automatically gives a closed equivalent system of equations.

- This approach forces one to introduce the scales for space and time, as well as separate scales for all variables and their gradients. Most of the terms will be characterized by the diffusive scaling, while for the remaining terms (mainly due to forcing), a simple rule will be adopted. The size of the force terms follows from the principle that a single term in an equation cannot be larger in size by one or several orders of magnitude than all other terms [35].

1. Diffusive scaling

First of all, a proper scaling must be introduced. In fact, note that the unit of space coordinate and that of time variable in Eq. (1) are the mean free path l_c and the mean collision time T_c, respectively. Obviously, they are not appropriate as the characteristic scales for flow field in the continuum limit. Let the characteristic length scale of the flow field be L and let the characteristic flow speed be U. There are two factors in the limit we are interested in. The continuum limit means $l_c \ll L$ and the low speed limit means $U \ll C$, where $C\,(= l_c/T_c)$ is the average modulus of the particle speed. In the following asymptotic

analysis, we introduce the other dimensionless variables, defined by

$$x_i = (l_c/L)\hat{x}_i, \qquad t = (UT_c/L)\hat{t}. \tag{19}$$

Defining the small parameter ϵ as $\epsilon = l_c/L$, which corresponds to the Knudsen number, we have $x_i = \epsilon\hat{x}_i$. Furthermore, assuming

$$U/C = \epsilon, \tag{20}$$

which is the key of derivation of the low Mach number limit [32], we have $t = \epsilon^2\hat{t}$. Then, Eq. (1) is rewritten as

$$\epsilon^2\frac{\partial f_\sigma}{\partial t} + \epsilon V_i\frac{\partial f_\sigma}{\partial x_i} = A_\sigma\left[f_{\sigma(*)} - f_\sigma\right] + d_\sigma, \tag{21}$$

In this new scaling, we can assume

$$\frac{\partial f}{\partial \alpha} = O(f), \qquad \frac{\partial \hat{m}}{\partial \alpha} = O(\hat{m}), \tag{22}$$

where $f = f_{\sigma(*)}, f_\sigma$ and $\alpha = t, x_i$ and $\hat{m} = \hat{\rho}_\sigma, \hat{q}_{\sigma i}$.

2. Grad moment system

The key point of this section is to derive the macroscopic equations and, consequently, the definitions of the recovered transport coefficients.

The matrix M can be used to compute some equilibrium moments. Let us introduce the general nomenclature for non-conserved equilibrium moments

$$\Pi^*_{11\cdots1\,22\cdots2}(\overbrace{11\cdots1}^{n\text{ times}}, \overbrace{22\cdots2}^{m\text{ times}}) = \langle V_1^n V_2^m f_{\sigma(*)}\rangle. \tag{23}$$

Recalling that the diffusive scaling implies $\hat{u}_{\sigma i} = \epsilon\, u_{\sigma i}$ and $\hat{u}^*_{\sigma i} = \epsilon\, u^*_{\sigma i}$, the moments defined

by means of the matrix M are

$$Mf_{\sigma(*)} = \begin{bmatrix} \Pi^*_0 \\ \Pi^*_1 \\ \Pi^*_2 \\ \Pi^*_{11} \\ \Pi^*_{22} \\ \Pi^*_{12} \\ \Pi^*_{221} \\ \Pi^*_{112} \\ \Pi^*_{1122} \end{bmatrix} = \begin{bmatrix} \hat{\rho}_\sigma \\ \epsilon\,\hat{\rho}_\sigma u^*_{\sigma 1} \\ \epsilon\,\hat{\rho}_\sigma u^*_{\sigma 2} \\ \hat{p}_\sigma + \epsilon^2\,\hat{\rho}_\sigma (u^*_{\sigma 1})^2 \\ \hat{p}_\sigma + \epsilon^2\,\hat{\rho}_\sigma (u^*_{\sigma 2})^2 \\ \epsilon^2\,\hat{\rho}_\sigma u^*_{\sigma 1} u^*_{\sigma 2} \\ \epsilon\,\hat{\rho}_\sigma u^*_{\sigma 1}/3 \\ \epsilon\,\hat{\rho}_\sigma u^*_{\sigma 2}/3 \\ \hat{p}_\sigma/3 + \epsilon^2\,\hat{\rho}_\sigma (u^*_{\sigma 1})^2/3 + \epsilon^2\,\hat{\rho}_\sigma (u^*_{\sigma 2})^2/3 \end{bmatrix}. \tag{24}$$

The previous nomenclature can be expressed for non-conserved generic moments as well, namely

$$\Pi_{11\cdots 1\,22\cdots 2}(\overbrace{11\cdots 1}^{n\text{ times}}, \overbrace{22\cdots 2}^{m\text{ times}}) = \langle V_1^n V_2^m f_\sigma \rangle. \tag{25}$$

We can now apply the asymptotic analysis of the MRT-LBM scheme based on the Grad moment system. Let us compute the first moments of the Eq. (21) (corresponding to the first three rows of the matrix M), namely

$$\frac{\partial \hat{\rho}_\sigma}{\partial t} + \frac{\partial (\hat{\rho}_\sigma u_{\sigma i})}{\partial x_i} = 0, \tag{26}$$

$$\begin{aligned} &\epsilon^3 \frac{\partial (\hat{\rho}_\sigma u_{\sigma i})}{\partial t} + \epsilon \frac{\partial \Pi_{i\,j}}{\partial x_j} = \lambda^\delta_\sigma (\Pi^*_i - \Pi_i) + \hat{\rho}_\sigma \hat{c}_{\sigma i} = \\ &= \epsilon\,\lambda^\delta_\sigma \hat{\rho}_\sigma (u^*_{\sigma i} - u_{\sigma i}) + \hat{\rho}_\sigma \hat{c}_{\sigma i} = \epsilon\,\hat{p} \sum_\varsigma B_{\sigma\varsigma}\,\hat{y}_\sigma \hat{y}_\varsigma (u_{\varsigma i} - u_{\sigma i}) + \hat{\rho}_\sigma \hat{c}_{\sigma i}, \end{aligned} \tag{27}$$

where $\hat{y}_\sigma = \hat{p}_\sigma/\hat{p}$ is the molar concentration and the relation $m\,\hat{x}_\sigma/m_\sigma = \hat{y}_\sigma$ has been used. In deriving the previous equations, the assumption given by Eq. (15) has been considered. First of all, it is worth the effort to point out that the previous equations are consistent with the macroscopic Maxwell–Stefan mass diffusion model [15]. Secondly if $u^*_{\sigma i} - u_{\sigma i} \sim O(1)$, i.e. the constant U properly characterizes the order of magnitude of the diffusion velocities too or, equivalently, the diffusion velocities are large, then necessarily $\hat{c}_{\sigma i} = \epsilon c_{\sigma i}$, because of the above–mentioned principle that a single term in an equation cannot be larger in size by one or several orders of magnitude than all other terms.

In the momentum equation, the stress tensor appears. We now search for simplified expressions of the stress tensor components. The equations for the stress tensor components involve higher order moments like Π_{ijk}. According to the assumed scaling, each moment dynamics is ruled first by its equilibrium part, in this case Π^*_{ijk}, namely

$$\Pi^*_{ijk} = \epsilon/3 \left(\delta_{ij}\hat{\rho}_\sigma u^*_{\sigma k} + \delta_{ki}\hat{\rho}_\sigma u^*_{\sigma j} + \delta_{jk}\hat{\rho}_\sigma u^*_{\sigma i}\right). \tag{28}$$

Clearly $\Pi^*_{ijk} \sim O(\epsilon)$, which means that the equilibrium part of these higher order moments is of the same order of the external forces or, equivalently, that we cannot neglect the terms due the external forces for designing a simplified expression for these higher order moments. Consequently, the leading part of the equations for the higher order moments yields

$$\Pi^*_{ijk} - \Pi_{ijk} + \epsilon\, \delta_{ij}\delta_{ki}\delta_{jk}\hat{\rho}_\sigma c_{\sigma i} \cong 0, \tag{29}$$

where the fact that the higher order relaxation frequencies have been assumed equal to one is used, or, equivalently,

$$\Pi_{ijk} \cong \epsilon/3 \left(\delta_{ij}\hat{\rho}_\sigma u^*_{\sigma k} + \delta_{ki}\hat{\rho}_\sigma u^*_{\sigma j} + \delta_{jk}\hat{\rho}_\sigma u^*_{\sigma i}\right) + \epsilon\, \delta_{ij}\delta_{ki}\delta_{jk}\hat{\rho}_\sigma c_{\sigma i}. \tag{30}$$

It is worth the effort to point out that the last term in the previous expression is an error due to the intrinsic lattice. In fact, for the D2Q9 lattice, the argument of the moment Π_{iii} (for any $i = 1, 2$) is identical to that of the hydrodynamic moment Π_i and this is an intrinsic drawback due to the fact that all the lattice velocity components in the D2Q9 lattice have modulus equal to one. Fortunately the second order moments of the forcing terms have been designed in such a way to compensate the intrinsic errors of the considered lattice. In fact, after substituting the previous simplifications, the equations for the stress tensor components yield

$$\epsilon^2\frac{\partial \Pi_{11}}{\partial t} + \epsilon\frac{\partial \Pi^*_{11\,k}}{\partial x_k} + \epsilon^2\frac{\partial(\hat{\rho}_\sigma c_{\sigma 1})}{\partial x_1} = \frac{\lambda^\xi_\sigma + \lambda^\nu_\sigma}{2}\left(\Pi^*_{11} - \Pi_{11}\right) + \frac{\lambda^\xi_\sigma - \lambda^\nu_\sigma}{2}\left(\Pi^*_{22} - \Pi_{22}\right) + \epsilon^2\frac{\partial(\hat{\rho}_\sigma c_{\sigma 1})}{\partial x_1}, \tag{31}$$

$$\epsilon^2\frac{\partial \Pi_{22}}{\partial t} + \epsilon\frac{\partial \Pi^*_{22\,k}}{\partial x_k} + \epsilon^2\frac{\partial(\hat{\rho}_\sigma c_{\sigma 2})}{\partial x_2} = \frac{\lambda^\xi_\sigma - \lambda^\nu_\sigma}{2}\left(\Pi^*_{11} - \Pi_{11}\right) + \frac{\lambda^\xi_\sigma + \lambda^\nu_\sigma}{2}\left(\Pi^*_{22} - \Pi_{22}\right) + \epsilon^2\frac{\partial(\hat{\rho}_\sigma c_{\sigma 2})}{\partial x_2}, \tag{32}$$

$$\epsilon^2\frac{\partial \Pi_{12}}{\partial t} + \epsilon\frac{\partial \Pi^*_{12\,k}}{\partial x_k} = \lambda^\nu_\sigma\left(\Pi^*_{12} - \Pi_{12}\right), \tag{33}$$

where, in the equations for the diagonal components, the terms due to the limits of the considered lattice have been redundantly reported, even though the design of the forcing term allows one to cancel them out.

Clearly from the previous equations, $\Pi_{ij} \cong \Pi^*_{ij} \cong \hat{p}_\sigma \delta_{ij}$ and this proves that $\hat{p}_\sigma \delta_{ij}$ is the leading term of the stress tensor and it can be used in estimating the first term in LHS of the previous equations. Moreover the advection terms of the LHS of the previous equations can be approximated by Eqs. (28). Finally the previous substitutions in terms of Π_{ij} yields

$$\Pi_{ij} \cong \hat{p}_\sigma \delta_{ij} + \epsilon^2 \hat{\rho}_\sigma u^*_{\sigma i} u^*_{\sigma j} - \frac{\epsilon^2}{3\,\lambda_\nu}\left[\frac{\partial(\hat{\rho}_\sigma u^*_{\sigma i})}{\partial x_j} + \frac{\partial(\hat{\rho}_\sigma u^*_{\sigma j})}{\partial x_i}\right] + \frac{\epsilon^2}{3}\left(\frac{1}{\lambda_\nu} - \frac{1}{\lambda_\xi}\right)\frac{\partial(\hat{\rho}_\sigma u^*_{\sigma k})}{\partial x_k}\delta_{ij}, \quad (34)$$

where the assumptions given by Eqs. (16,17) have been considered. Taking the divergence of the previous tensor yields

$$\frac{\partial \Pi_{ij}}{\partial x_j} \cong \frac{\partial \hat{p}_\sigma}{\partial x_i} + \epsilon^2 \frac{\partial}{\partial x_j}(\hat{\rho}_\sigma u^*_{\sigma i} u^*_{\sigma j}) - \frac{\epsilon^2}{3\,\lambda_\nu}\frac{\partial^2(\hat{\rho}_\sigma u^*_{\sigma i})}{\partial x_j^2} - \frac{\epsilon^2}{3\,\lambda_\xi}\frac{\partial^2(\hat{\rho}_\sigma u^*_{\sigma k})}{\partial x_i \partial x_k} \quad (35)$$

Introducing Eq. (35) into Eq. (27) yields

$$\begin{aligned}
&\epsilon^2\left[\frac{\partial(\hat{\rho}_\sigma u_{\sigma i})}{\partial t} + \frac{\partial}{\partial x_j}(\hat{\rho}_\sigma u^*_{\sigma i} u^*_{\sigma j}) - \frac{1}{3\,\lambda_\nu}\frac{\partial^2(\hat{\rho}_\sigma u^*_{\sigma i})}{\partial x_j^2} - \frac{1}{3\,\lambda_\xi}\frac{\partial^2(\hat{\rho}_\sigma u^*_{\sigma k})}{\partial x_i \partial x_k}\right] = \\
&= -\frac{\partial \hat{p}_\sigma}{\partial x_i} + \hat{p}\sum_\varsigma B_{\sigma\varsigma}\,\hat{y}_\sigma \hat{y}_\varsigma (u_{\varsigma i} - u_{\sigma i}) + \hat{\rho}_\sigma c_{\sigma i}. \quad (36)
\end{aligned}$$

The previous equation allows one to discuss the proper scaling for the pressure $\hat{p}_\sigma$. Clearly two sets of terms exist in the previous equation: the leading terms $\sim O(1)$ which describe the mass diffusion (according to the Maxwell–Stefan model) and the terms $\sim O(\epsilon^2)$ which describe the viscous phenomena. Hence the most general expression for the single component pressure is $\hat{p}_\sigma = p_\sigma + \epsilon^2 p'_\sigma$ (similar considerations lead to $\hat{\rho}_\sigma = \rho_\sigma + \epsilon^2 \rho'_\sigma$ as well). With other words, it is possible to imagine that the single component pressure field $\hat{p}_\sigma$ is due to two contributions: a *slow* dynamics mainly driven by the diffusion process p_σ and a *fast* dynamics driven by the viscous phenomena p'_σ. Moreover it makes sense to assume that the external field which discriminates among the particle nature, i.e. $\hat{b}_{\sigma i}$, produces a term with the same order of magnitude of those describing the diffusion phenomenon, while the external field constant for all the components affects the viscous phenomena only, i.e. $c_{\sigma i} = \epsilon^2 a_i + b_{\sigma i}$. This implies that the terms depending on the spatial gradients in the forcing definition given by Eq. (18) are required by $b_{\sigma i}$, which is the leading part. In case of a_i only, the corresponding force (in lattice units) is so small that no correction is required [31]. These considerations lead to

$$\frac{\partial \rho_\sigma}{\partial t} + \frac{\partial(\rho_\sigma u_{\sigma i})}{\partial x_i} = 0, \quad (37)$$

$$\frac{\partial y_\sigma}{\partial x_i} = \sum_\varsigma B_{\sigma\varsigma}\, y_\sigma y_\varsigma (u_{\varsigma i} - u_{\sigma i}) + \frac{\rho_\sigma b_{\sigma i}}{p}, \tag{38}$$

$$\frac{\partial(\rho_\sigma u_{\sigma i})}{\partial t} + \frac{\partial}{\partial x_j}(\rho_\sigma u^*_{\sigma i} u^*_{\sigma j}) + \frac{\partial p'_\sigma}{\partial x_i} = \frac{1}{3\,\lambda_\nu}\frac{\partial^2(\rho_\sigma u^*_{\sigma i})}{\partial x_j^2} + \frac{1}{3\,\lambda_\xi}\frac{\partial^2(\rho_\sigma u^*_{\sigma k})}{\partial x_i \partial x_k} + \rho_\sigma a_i. \tag{39}$$

Clearly summing Eq. (38) over all the components σ yields $\sum_\sigma \rho_\sigma b_{\sigma i} = 0$, which means that large external fields acting at the leading diffusion level are possible, as far as their net effect is zero (otherwise the large net effect would produce accelerations which are not compatible with the low Mach number limit). Summing over the components yields

$$\frac{\partial \rho}{\partial t} + \frac{\partial(\rho u_i)}{\partial x_i} = 0, \tag{40}$$

$$\frac{\partial(\rho u_i)}{\partial t} + \frac{\partial}{\partial x_j}\sum_\sigma(\rho_\sigma u^*_{\sigma i} u^*_{\sigma j}) + \frac{\partial p'}{\partial x_i} = \frac{1}{3\,\lambda_\nu}\frac{\partial^2(\rho u_i)}{\partial x_j^2} + \frac{1}{3\,\lambda_\xi}\frac{\partial^2(\rho u_k)}{\partial x_i \partial x_k} + \rho a_i, \tag{41}$$

where $p' = \sum_\sigma p'_\sigma$ and the Property 2 has been applied. Clearly there is no equation for $\rho = \sum_\sigma \rho_\sigma$, which means that this quantity is an arbitrary constant. This means that, at the leading diffusion level, density fields characterized by large concentration gradients are possible, as far as their net effect is a nearly constant total density field (otherwise again the non-smooth total density field would produce accelerations which are not compatible with the low Mach number limit). Since ρ is a constant, then the previous expressions can be simplified as

$$\frac{\partial u_i}{\partial x_i} = 0, \tag{42}$$

$$\frac{\partial u_i}{\partial t} + \frac{\partial}{\partial x_j}\sum_\sigma(x_\sigma u^*_{\sigma i} u^*_{\sigma j}) + \frac{1}{\rho}\frac{\partial p'}{\partial x_i} = \nu\,\frac{\partial^2 u_i}{\partial x_j^2} + a_i. \tag{43}$$

Clearly the previous equations are not the canonical Navier–Stokes system of equations for the barycentric velocity u_i, because of the complex advection term in the momentum equation. This is not due to the adopted asymptotic analysis based on the Grad moment system. The same result would be obtained by using the Hilbert expansion: see for example Ref. [25]. If and only if the component particles have similar masses, i.e. $m_\sigma \cong m$, then $u^*_{\sigma i} \cong u_i$ because of Property 1 and the previous momentum equation reduces to

$$\frac{\partial u_i}{\partial t} + u_j\frac{\partial u_i}{\partial x_j} + \frac{1}{\rho}\frac{\partial p'}{\partial x_i} = \nu\,\frac{\partial^2 u_i}{\partial x_j^2} + a_i. \tag{44}$$

In this section, the macroscopic equations due to the proposed MRT-LBM scheme with forcing were derived. The model is consistent with (a) the Maxwell–Stefan diffusion model

and (b), in case of particles with similar masses, it allows one to recover a Navier–Stokes system of equations for the mixture barycentric quantities, with a tunable mixture viscosity. Additionally (c) two types of forces are considered: the first one which produces zero net effect at the mixture level and the second which produces a global effect which is compatible with the low Mach number limit.

C. Efficient numerical implementation

In the previous sections, the space–time discretization has not been discussed. It is well known that it is very convenient to discretize the LBM schemes along the characteristics, i.e. along the lattice velocities, because they are constant and analytical known. However the popular forward Euler integration rule can not be applied in this case because it leads to a lack of mass conservation [25]. Consequently a more accurate scheme must be considered: for example, the second-order Crank–Nicolson rule is enough in order to avoid this problem. Let us use this rule to discretize Eq. (1), namely

$$f_\sigma^+ = f_\sigma + (1-\theta)\, A_\sigma \left[f_{\sigma(*)} - f_\sigma \right] + \theta\, A_\sigma^+ \left[f_{\sigma(*)}^+ - f_\sigma^+ \right] + (1-\theta)\, d_\sigma + \theta\, d_\sigma^+, \tag{45}$$

where the argument (t, x_i) is omitted and the functions computed in $(t+\epsilon^2, x_i + \epsilon\, V_i)$ are identified by the superscript $+$. The Crank–Nicolson rule is recovered for $\theta = 1/2$. The previous formula would force one to consider quite complicated integration procedures [25]. Fortunately a simple variable transformation has been already proposed in order to simplify this task [38], and successfully applied in case of mixtures [16]. This procedure has been already generalized in case of the MRT formulation [39].

Let us introduce a local transformation

$$g_\sigma = f_\sigma - \theta\, A_\sigma \left[f_{\sigma(*)} - f_\sigma \right] - \theta\, d_\sigma. \tag{46}$$

Substituting the transformation given by Eq. (46) into Eq. (45) yields

$$g_\sigma^+ = g_\sigma + A_\sigma \left(I + \theta\, A_\sigma \right)^{-1} \left[f_{\sigma(*)} - g_\sigma \right] + \left(I + \theta\, A_\sigma \right)^{-1} d_\sigma, \tag{47}$$

where it is worth the effort to remark that the local equilibrium remains unchanged. Essentially the algorithm consisists of (a) appling the previous transformation $f_\sigma \to g_\sigma$ defined by Eq. (46), then (b) computing the collision and streaming step $g_\sigma \to g_\sigma^+$ by means of the

formula given by Eq. (47) and finally (c) coming back to the original discrete distribution function $g_\sigma^+ \rightarrow f_\sigma^+$. The problem, in case of mixtures, arises from the last step. In fact, the formula required in order to perform the last task (c) is

$$f_\sigma^+ = \left(I + \theta\, A_\sigma^+\right)^{-1} \left[g_\sigma^+ + \theta\, A_\sigma^+ f_{\sigma(*)}^+ + \theta\, d_\sigma^+\right]. \tag{48}$$

Since d_σ depends in general on spatial gradients, it may be not very simple to compute d_σ^+ at the new time step, because some of the neighboring values may be not available. Hence the following assumption is considered $d_\sigma^+ \approx d_\sigma(t, x_i + \epsilon\, V_i)$ leading to the final formula

$$f_\sigma^+ = \left(I + \theta\, A_\sigma^+\right)^{-1} \left[g_\sigma^+ + \theta\, A_\sigma^+ f_{\sigma(*)}^+ + \theta\, d_\sigma(t, x_i + \epsilon\, V_i)\right]. \tag{49}$$

In order to compute both A_σ^+ (depending on total pressure and total density) and $f_{\sigma(*)}^+$, the updated hydrodynamic moments, i.e. the hydrodynamic moments at the new time step, are required. Since the single component density is conserved, recalling Eq. (46) yields

$$\hat{\rho}_\sigma^+ = \langle g_\sigma^+ \rangle, \tag{50}$$

consequently it is possible to compute $\hat{p}_\sigma^+$, $\hat{\rho}^+$, $\hat{p}^+$ and finally A_σ^+.

However this is not the case for the single component momentum, because this is not a conserved quantity and hence the first order moments for g_σ^+ and f_σ^+ differ [16]. Recalling Eq. (46) and taking the first order moment of it yields

$$\begin{aligned} \langle V_i\, g_\sigma^+ \rangle &= \hat{\rho}_\sigma^+ \hat{u}_{\sigma i}^+ - \theta\, \lambda_\sigma^{\delta+} \hat{\rho}_\sigma^+ (\hat{u}_{\sigma i}^{*+} - \hat{u}_{\sigma i}^+) - \theta\, \hat{\rho}_\sigma^+ \hat{c}_{\sigma i}^+ = \\ &= \hat{\rho}_\sigma^+ \hat{u}_{\sigma i}^+ - \theta\, \hat{p}^+ \sum_\varsigma B_{\sigma\varsigma}\, \hat{y}_\sigma^+ \hat{y}_\varsigma^+ (\hat{u}_{\varsigma i}^+ - \hat{u}_{\sigma i}^+) - \theta\, \hat{\rho}_\sigma^+ \hat{c}_{\sigma i}^+. \end{aligned} \tag{51}$$

It is worth the effort to point out an important property. Summing the previous equations for all the components yields

$$\hat{q}_i^+ = \hat{\rho}^+ \hat{u}_i^+ = \sum_\sigma \langle V_i\, g_\sigma^+ \rangle + \theta \sum_\sigma \hat{\rho}_\sigma^+ \hat{c}_{\sigma i}^+, \tag{52}$$

which means that it is possible to compute $\hat{\rho}^+ \hat{u}_i^+$ directly by means of g_σ^+. For this reason, it is possible to consider a simplified procedure in case of particles with similar masses.

1. *Particles with similar masses*

In case of particles with similar masses, $\hat{u}_{\sigma i}^{*+} \cong \hat{u}_i^+$ and Eq. (51) reduces to

$$\langle V_i\, g_\sigma^+ \rangle \cong \hat{\rho}_\sigma^+ \hat{u}_{\sigma i}^+ - \theta\, \lambda_\sigma^{\delta+} \hat{\rho}_\sigma^+ (\hat{u}_i^+ - \hat{u}_{\sigma i}^+) - \theta\, \hat{\rho}_\sigma^+ \hat{c}_{\sigma i}^+, \tag{53}$$

and equivalently, by taking into account Eq. (52),

$$\hat{\rho}_\sigma^+ \hat{u}_{\sigma i}^+ \cong \frac{\langle V_i\, g_\sigma^+\rangle + \theta\, \hat{\rho}_\sigma^+ \hat{c}_{\sigma i}^+ + \theta\, \lambda_\sigma^{\delta+} \hat{x}_\sigma^+ \left(\sum_\sigma \langle V_i\, g_\sigma^+\rangle + \theta \sum_\sigma \hat{\rho}_\sigma^+ \hat{c}_{\sigma i}^+\right)}{1 + \theta\, \lambda_\sigma^{\delta+}}. \tag{54}$$

Actually the situation is even simpler, bacause the previous formula is not needed. In fact, if $\hat{u}_{\sigma i}^{*+} \cong \hat{u}_i^+$, it is enough $\hat{u}_i^+$ by Eq. (52) to compute $f_{\sigma(*)}^+$ for the back transformation given by Eq. (49).

2. Particles with different masses

In the general case, Eq. (51) can be recasted as

$$\langle V_i\, g_\sigma^+\rangle = \hat{q}_{\sigma i}^+ - \theta\, \lambda_\sigma^{\delta+} \sum_\varsigma \chi_{\sigma\varsigma}\, (\hat{x}_\sigma^+ \hat{q}_{\varsigma i}^+ - \hat{x}_\varsigma^+ \hat{q}_{\sigma i}^+) - \theta\, \hat{\rho}_\sigma^+ \hat{c}_{\sigma i}^+, \tag{55}$$

where $\hat{q}_{\sigma i}^+ = \hat{\rho}_\sigma^+ \hat{u}_{\sigma i}^+$ and

$$\chi_{\sigma\varsigma} = \frac{m^2}{m_\sigma m_\varsigma} \frac{B_{\sigma\varsigma}}{B_{m\,m}}. \tag{56}$$

Clearly $\chi_{\sigma\varsigma}$ is a symmetric matrix. Finally, grouping together common terms yields

$$\langle V_i\, g_\sigma^+\rangle + \theta\, \hat{\rho}_\sigma^+ \hat{c}_{\sigma i}^+ = \left[1 + \theta\, \lambda_\sigma^{\delta+} \sum_\varsigma (\chi_{\sigma\varsigma}\, \hat{x}_\varsigma^+)\right] \hat{q}_{\sigma i}^+ - \theta\, \lambda_\sigma^{\delta+}\, \hat{x}_\sigma^+ \sum_\varsigma (\chi_{\sigma\varsigma}\, \hat{q}_{\varsigma i}^+). \tag{57}$$

Clearly the previous expression defines a liner system of algebraic equations for the unknowns $\hat{q}_{\sigma i}^+$. This means that in order to compute the updated values for all $\hat{q}_{\sigma i}^+$ a linear system of equations must be solved in terms of known quantities $\langle V_i\, g_\sigma^+\rangle$. It is possible to verify analytically (for few components) that the solvability condition of the previous linear system is always ensured, for any combination of mass concentrations and Maxwell–Stefan resistances. However a general mathematical proof for any number of components is currently missing. Note that this eventual restriction of the discussed scheme would be a constraint of the proposed numerical implementation and not of the kinetic model itself. The possibility to tune θ is not available, because all the schemes for $\theta \neq 1/2$ may imply a lack of mass conservation.

In the degenerate case $\chi_{\sigma\varsigma} = 1$, i.e. particles with equal masses, Eq. (57) reduces to

$$\langle V_i\, g_\sigma^+\rangle + \theta\, \hat{\rho}_\sigma^+ \hat{c}_{\sigma i}^+ = \left(1 + \theta\, \lambda_\sigma^{\delta+}\right) \hat{q}_{\sigma i}^+ - \theta\, \lambda_\sigma^{\delta+}\, \hat{x}_\sigma^+ \hat{q}_i^+, \tag{58}$$

which is equivalent to Eq. (54).

In the next section, the results for some numerical simulations are reported.

III. NUMERICAL SIMULATIONS

The main improvement discussed in the present paper with regards to previous work [15] lies in the possibility to control the higher order viscous dynamics independently on the diffusion phenomenon. The Schmidt number, i.e. the ratio between the mixture viscosity and the Fick diffusion coefficient $\mathsf{Sc} = \nu/D$, is sometimes used to characterize the relative magnitude of the previous phenomena, in the limiting cases for which the generalized Fick model applies. The numerical simulations reported in this section aim (1) to prove this feature, i.e. the possibility to tune the Schmidt number, and (2) to find out the stability and accuracy region of the proposed scheme.

First of all, it is important to point out that the Schmidt number intrinsically refers to a Fickian diffusion regime, where a single diffusion coefficient D for a generic species can be defined. In some limiting cases, the Maxwell–Stefan diffusion model automatically reduces to the Fick model with a proper diffusion coefficient depending on the local concentrations. Following [15], the solvent limiting case [40, 41] will be considered and a standard procedure for measuring the diffusion transport coefficients [26, 42] will be adopted.

Let us consider a ternary mixture realizing a Poiseuille flow, i.e. a 2D flow between two parallel plates oriented along the direction of the x_1–axis of the reference system. The computational domain is defined by $(t, x_1, x_2) \in [0, T] \times [0, L_1] \times [0, L_2]$. The average mixture transport of the barycentric velocity is ruled by Eqs. (42, 43), which clearly depend on the external force. For the sake of simplicity, only the term effecting the mixture barycentric velocity will be considered, with $a_1 = 0.001$ and $a_2 = 0$, while the term which discriminates among the particle nature will be neglected, i.e. $b_{\sigma i} = 0$. Assuming $u_2 = 0$ and p' constant, Eq. (43) admits, in steady state conditions, the following solution

$$u_1(x_2) - u_1(0) = \frac{a_1 \, L_2^2}{2 \, \nu} \, \frac{x_2}{L_2} \left(1 - \frac{x_2}{L_2} \right). \tag{59}$$

It is possible to use the previous analytical solution to derive a numerical measure of the kinematic viscosity realized by the scheme. Introducing $x_M = x_1(L_2/2)$ and $x_0 = x_1(0)$ yields

$$\nu^* = \left\| \frac{a_1 \, L_2^2}{8 \, (u_M - u_0)} \right\|, \tag{60}$$

where $\|\cdot\|$ is a spatial average on the domain $[0, L_1] \times [0, L_2]$. The measured kinematic viscosity ν^* may differ from the theoretical one $\nu \in [1, 20]$, because of the numerical errors.

Concerning the diffusion phenomenon, the molecular weights of the components in the ternary mixture are $m_\sigma = [1, 2, 3]$ and consequently the corrective factors are $\varphi_\sigma = [1, 1/2, 1/3]$. The theoretical Maxwell–Stefan diffusion resistance is given by

$$B_{\sigma\varsigma} = \beta \left(\frac{1}{m_\sigma} + \frac{1}{m_\varsigma} \right)^{-1/2}, \tag{61}$$

where $\beta \in [5, 166]$. Let us suppose that in our ternary mixture the component 3 is a *solvent*, i.e. its concentration is predominant in comparison with the other components of the mixture. Hence $y_3 \cong 1$ and consequently $y_1 \cong 0$ and $y_2 \cong 0$. Under these assumptions, Eq. (38) reduce to

$$\nabla y_1 \cong B_{13} y_1 y_3 (u_3 - u_1) \cong B_{13} y_1 (v - u_1), \tag{62}$$

$$\nabla y_2 \cong B_{23} y_2 y_3 (u_3 - u_2) \cong B_{23} y_2 (v - u_2), \tag{63}$$

where the last simplification assumes $v = \sum_\varsigma y_\varsigma u_\varsigma \cong u_3$. Consequently the measured diffusion resistances are given by

$$B^*_{13} = \frac{1}{D^*_1} = \left\| \frac{\partial y_1 / \partial x}{y_1 (v - u_1)} \right\|, \tag{64}$$

$$B^*_{23} = \frac{1}{D^*_2} = \left\| \frac{\partial y_2 / \partial x}{y_2 (v - u_2)} \right\|, \tag{65}$$

where $D^*_1 = 1/B^*_{13}$ and $D^*_2 = 1/B^*_{23}$ are the measured Fick diffusion coefficients for the non-solvent components. Combining the viscous and the diffusion phenomena, it is possible to introduce the Schmidt numbers for the non-solvent components as well, i.e. $\mathsf{Sc}^*_1 = \nu^*/D^*_1 = \nu^* B^*_{13}$ and $\mathsf{Sc}^*_2 = \nu^*/D^*_2 = \nu^* B^*_{23}$.

Concerning the boundary conditions, at the inlet ($x_1 = 0$) and outlet ($x = L_1$) of the computational domain, the periodic boundary conditions apply. At the wall, for sake of simplicity, the incoming (unknown) components of the single-species distribution functions $f_{\sigma i}$ are assumed equal to the corresponding components of the equilibrium distribution functions with zero velocity, namely $f^n_{\sigma i} = \rho^n_\sigma w_i s_{\sigma i}$, where the density ρ^n_σ is extrapolated from the bulk along the normal direction. It is well known that this simple boundary condition produces (unphysical) numerical velocity slip at the wall. However this drawback does not affect the accuracy of the measured transport coefficients, if the numerical slip is properly taken into account, as reported in Eq. (60). For practical simulations, more advanced wall boundary conditions [43, 44] should be considered.

The initial velocity fields are zero for all the species, i.e. $u_{\sigma i}(0, x_1, x_2) = 0$ for all the species. On the other hand, the initial conditions for the partial pressures are given by

$$p_1(0, x_1, x_2) = \Delta p \left[1 + \sin\left(2\pi \frac{x_1}{L_1}\right)\right] + p_s, \tag{66}$$

$$p_2(0, x_1, x_2) = \Delta p \left[1 + \cos\left(2\pi \frac{x_1}{L_1}\right)\right] + p_s, \tag{67}$$

$$p_3(0, x_1, x_2) = 1 - p_1(0, x_1, x_2) - p_2(0, x_1, x_2), \tag{68}$$

where, for the reported numerical simulations, $\Delta p = p_s = 0.01$. The parameter p_s is a small pressure shift in order to avoid divisions by zero in computing the velocity by the corresponding momentum.

The spatial discretization step is called $\delta x = \delta x_1 = \delta x_2$ and the total number of grid points is $N_1 = L_1/\delta x = 60$ and $N_2 = L_2/\delta x = 40$. Similarly the time discretization step is selected in such a way that $\delta t \sim \delta x$ in order to have $c = \delta x/\delta t = 1$, and in particular $N_t = T/\delta t = 600$.

In Figure 1 and 2, the iso-contours of the molar concentrations y_1 and y_2 at the time step $t = T = 600\,\delta t$ in the domain $[0, L_1] \times [0, L_2]$ are reported. Clearly the mixture barycentric velocity produces a global transport on the right (along the direction of the x_1–axis), which is maximum at the center of the gap between the two plates and minimum at the wall (slip condition was assumed), because of the external applied force. Recalling the initial conditions given by Eqs. (66) and checking the positions of the maximum values in the concentration profiles, the transport at the center of the gab leads to a shift on the right roughly equal to $L_1/4$. Looking closer to the numerical solutions, the width of the iso-contour corresponding to the molar concentration equal to 0.026 is clearly narrower for the species 1 than for the species 2. This means that the value 0.026 is closer to the maximum of y_1 (0.0263) than the maximum of y_2 (0.0270), or, with other words, that the diffusion of the species 1 is proceeding faster than that of the species 2 from the common initial value (0.030) toward the common equilibrium value (0.020). This makes sense because the assumed transport coefficients imply $B_{13} < B_{23}$, which means a smaller diffusion resistance for the species 1.

Let us check the transport coefficients, effectively recovered by the numerical scheme. In Figure 3, the comparison between the numerical kinematic viscosity and the theoretical one is reported. Clearly the results are very good on the whole range of considered Maxwell–Stefan diffusion resistances. This means that the diffusion phenomena are not effecting

much the viscous phenomena and this could suggest one that a strong separation among the characteristic scales exist.

Unfortunately the opposite consideration is not correct. In Figure 4 and Figure 5, the theoretical values for the Maxwell–Stefan diffusion resistances are compared with the measured values. For high values of the Maxwell–Stefan resistances, an effect of the kinematic viscosity appears, in particular, in case of low viscosity, which means high Reynolds numbers. This means that, in order to reduce the numerical error on the diffusion phenomena, the Reynolds number should be as small as possible (or the dimensionless viscosity should be as large as possible). The situation is worst for the species 2, because $\varphi_2 = 1/2 < 1$ has been considered in order to take into account the proper molecular weight. The correction works fine, but it reduces the accuracy in case of non-negligible Reynolds numbers. Finally for small Maxwell–Stefan resistances, the situation is not clear, because of the overlapping of the plotted curves.

For achieving a better insight of the situation, a more systematic simulation campaign was designed. Let us consider the following sets of (logarithmically spanned) values for the parameters ν and β respectively

$$\begin{aligned}\Gamma_\nu \;=\; \{&1.00, 1.17, 1.37, 1.60, 1.88, 2.20, 2.58, 3.02, 3.53, 4.13, \ldots \\ &\ldots 4.84, 5.67, 6.63, 7.77, 9.09, 10.64, 12.46, 14.59, 17.08, 20.00\},\end{aligned} \tag{69}$$

$$\begin{aligned}\Gamma_\beta \;=\; \{&5.00, 6.01, 7.23, 8.70, 10.46, 12.57, 15.12, 18.18, 21.87, 26.30, 31.62 \ldots \\ &\ldots 38.03, 45.73, 54.99, 66.13, 79.53, 95.64, 115.01, 138.30, 166.31\},\end{aligned} \tag{70}$$

where the latter together with Eq. (61) implies

$$\begin{aligned}\Gamma_{B13} \;=\; \{&4.33, 5.21, 6.26, 7.53, 9.06, 10.89, 13.10, 15.75, 18.94, 22.77, 27.39, 32.93, \ldots \\ &\ldots 39.60, 47.63, 57.27, 68.87, 82.82, 99.60, 119.77, 144.03\},\end{aligned} \tag{71}$$

$$\begin{aligned}\Gamma_{B23} \;=\; \{&5.48, 6.59, 7.92, 9.53, 11.45, 13.77, 16.56, 19.92, 23.95, 28.81, 34.64, 41.66, \ldots \\ &\ldots 50.10, 60.24, 72.44, 87.12, 104.76, 125.98, 151.50, 182.19\}.\end{aligned} \tag{72}$$

Let us consider a simulation campaign $\Gamma = \{\nu \in \Gamma_\nu \wedge \beta \in \Gamma_\beta\}$, which is composed by $20 \times 20 = 400$ runs. For each numerical simulation, all the meaningful transport coefficients

(ν^*, B^*_{13}, B^*_{23}) are measured. Clearly the larger errors are obtained for the measured Schmidt numbers, Sc^*_1 and Sc^*_2, because the latter come from the product of the elementary transport coefficients. The numerical results are reported by matrix form in Figure 6 and 7 for Sc^*_1 and Sc^*_2 respectively. Every time that the numerical error is lower than 10 %, the correspoding combination of trasport coefficients is marked as acceptable for the scheme. This constraint, when applied to Sc^*_2 is more restrictive than when applied to Sc^*_1. This confirms that taking into account different molecular weights by $\varphi_\sigma < 1$ may show some limits, in case of large mass ratios. On the same plots, the theoretical values of the Schmidt numbers are reported by some proper iso-values in the ranges $\mathsf{Sc}_1 \in [4.3, 2880.6]$ and $\mathsf{Sc}_2 \in [5.5, 3643.7]$ respectively. In order to ensure the desired accuracy for both the transport coefficients for any combination, the Schmidt numbers must be quite large: for this particular application, they should be roughly larger than 1000.

Clearly from the numerical point of view, the separation of the characteristic scales, which was assumed in the development of the scheme, works only asymptotically and the stability/accuracy issues may reduce the actual applicability of scheme to a constrained range of theoretical transport coefficients, depending on the considered application. By the way, this situation is common to most of lattice Boltzmann schemes.

IV. CONCLUSIONS

A new LBM scheme for homogeneous mixture modeling, based on the multiple–relaxation–time (MRT) formulation, which fully recovers Maxwell–Stefan diffusion model in the continuum limit with (a) external force and (b) tunable Schmidt number, was developed. This formulation allows one to tune the relaxation frequencies of the collisional matrix independently each other, and, in particular for the present application, it allows one to tune the mixture kinematic viscosity independently on the Maxwell–Stefan diffusion resistances. This is part of an on-going effort to improve existing LBM scheme for homogeneous mixtures. The same author already proposed a new scheme based on the theoretical basis of a recently proposed BGK-type kinetic model for gas mixtures [21], which used only one relaxation parameter. The actual MRT formulation substantially extended the applicability of the previous model.

The numerical simulations for the solvent test case with external force, confirmed the

validity of the proposed formulation and they allowed us to find out the numerical ranges for the transport coefficients, which ensure acceptable accuracies. The numerical results prove a contraction of the theoretical expectations, which were based on a strong separation among the characteristic scales. Essentially the Schmidt number needs to be large enough to ensure acceptable results.

Acknowledgments

The author would like to thank prof. Li-Shi Luo of Old Dominion University (USA) and prof. Taku Ohwada of Kyoto University (Japan) for many enlightening discussions concerning the kinetic equations for mixtures and the asymptotic analysis of kinetic equations respectively. Moreover he would like to thank dr. Ilya Karlin of ETH-Zurich (Switzerland) for pointing out the new results reported in Ref. [16] and Lin Zheng of Huazhong University of Science and Technology (China) for pointing out how to select λ_σ^δ in such a way that $\chi_{\sigma\varsigma}$ is symmetric.

---

[1] G. R. McNamara and G. Zanetti, Phys. Rev. Lett. **61**, 2332 (1988).

[2] F. J. Higuera and J. Jiménez, Europhys. Lett. **9**, 663 (1989).

[3] F. J. Higuera, S. Succi, and R. Benzi, Europhys. Lett. **9**, 345 (1989).

[4] H. Chen, S. Chen, and W. Matthaeus, Phys. Rev. A **45**, R5339 (1992).

[5] Y. Qian, D. d'Humières, and P. Lallemand, Europhys. Lett. **17**, 479 (1992).

[6] X. He and L.-S. Luo, Phys. Rev. E **55**, R6333 (1997).

[7] X. Shan and X. He, Phys. Rev. Lett. **80**, 65 (1998).

[8] M. Ancona, J. Computat. Phys. **115**, 107 (1994).

[9] M. Junk, Numer. Methods Part. Diff. Eq. **17**, 383 (2001).

[10] R. Benzi, S. Succi, and M. Vergassola, Phys. Rep. **222**, 145 (1992).

[11] S. Chen and G. D. Doolen, Annu. Rev. Fluid Mech. **30**, 329 (1998).

[12] G. D. Doolen (Editor), ed., *Lattice Gas Methods for Partial Differential Equations* (Addison-Wesley, New York, 1990).

[13] D. Wolf-Gladrow, *Lattice-Gas Cellular Automata and Lattice Boltzmann Models*, no. 1725 in

Lecture Notes in Mathematics (Springer-Verlag, Berlin, 2000), 2nd ed.

[14] S. Succi, *The Lattice Boltzmann Equation for Fluid Dynamics and Beyond* (Oxford University Press, New York, 2001), 2nd ed.

[15] P. Asinari (2008), submitted to Phys. Rev. E.

[16] S. Arcidiacono, I. V. Karlin, J. Mantzaras, and C. E. Frouzakis, Phys. Rev. E **76**, 046703 (2007).

[17] B. B. Hamel, Phys. Fluids **8**, 418 (1965).

[18] B. B. Hamel, Phys. Fluids **9**, 12 (1966).

[19] F. Williams, *Combustion Theory* (Benjamin/Cumming, California, 1986).

[20] V. Garzò, A. dos Santos, and J. J. Brey, Phys. Fluids A **1**, 380 (1989).

[21] P. Andries, K. Aoki, and B. Perthame, J. Stat. Phys. **106**, 993 (2002).

[22] J. C. Maxwell, Philos. Trans. R. Soc. **157**, 26 (1866).

[23] E. P. Gross and M. Krook, Phys. Rev. **102**, 593 (1956).

[24] P. L. Bhatnagar, E. P. Gross, and M. Krook, Phys. Rev. **94**, 511 (1954).

[25] P. Asinari, Phys. Rev. E **73**, 056705 (2006).

[26] M. E. McCracken and J. Abraham, Phys. Rev. E **71**, 046704 (2005).

[27] D. d'Humières, in *Rarefied Gas Dynamics: Theory and Simulations*, edited by B. D. Shizgal and D. P. Weave (AIAA, Washington, D.C., 1992), vol. 159 of *Prog. Astronaut. Aeronaut.*, pp. 450–458.

[28] P. Lallemand and L.-S. Luo, Phys. Rev. E **61**, 6546 (2000).

[29] D. d'Humières, I. Ginzburg, M. Krafczyk, P. Lallemand, and L.-S. Luo, Philos. Trans. R. Soc. Lond. A **360**, 437 (2002).

[30] P. Asinari, Phys. Fluids **17**, 067102 (2005).

[31] M. Junk, A. Klar, and L.-S. Luo, J. Computat. Phys. **210**, 676 (2005).

[32] Y. Sone, *Kinetic Theory and Fluid Dynamics* (Birkhäuser, Boston, 2002), 2nd ed.

[33] H. Struchtrup, *Macroscopic Transport Equations for Rarefied Gas Flows – Approximation Methods in Kinetic Theory*, Interaction ofMechanics andMathematics Series (Springer, Heidelberg, 2005).

[34] P. Asinari and T. Ohwada (2008), submitted to Comput. Math. Appl.

[35] H. Struchtrup, J. Stat. Phys. **125**, 565 (2006).

[36] H. Struchtrup, Phys. Fluids **16**, 3921 (2004).

[37] H. Struchtrup, Multiscale Model. Simul. **3**, 211 (2004).

[38] Z. L. Guo and T. S. Zhao, Phys. Rev. E **67**, 066709 (2003).

[39] A. Bardow, I. Karlin, and A. Gusev, Europhys. Lett. **75**, 434 (2006).

[40] W. S. R.B. Bird and E. Lightfoot, *Transport Phenomena* (John Wiley & Sons, New York, 1960).

[41] C. Brennen, *Fundamentals of Multiphase Flow* (Cambridge University Press, United Kingdom, 2005).

[42] E. G. Flekkoy, Phys. Rev. E **47**, 4247 (1993).

[43] I. Ginzburg and D. d'Humières, Phys. Rev. E **68**, 066614 (2003).

[44] M. Junk and Z. Yang, J. Stat. Phys. **121**, 3 (2005).

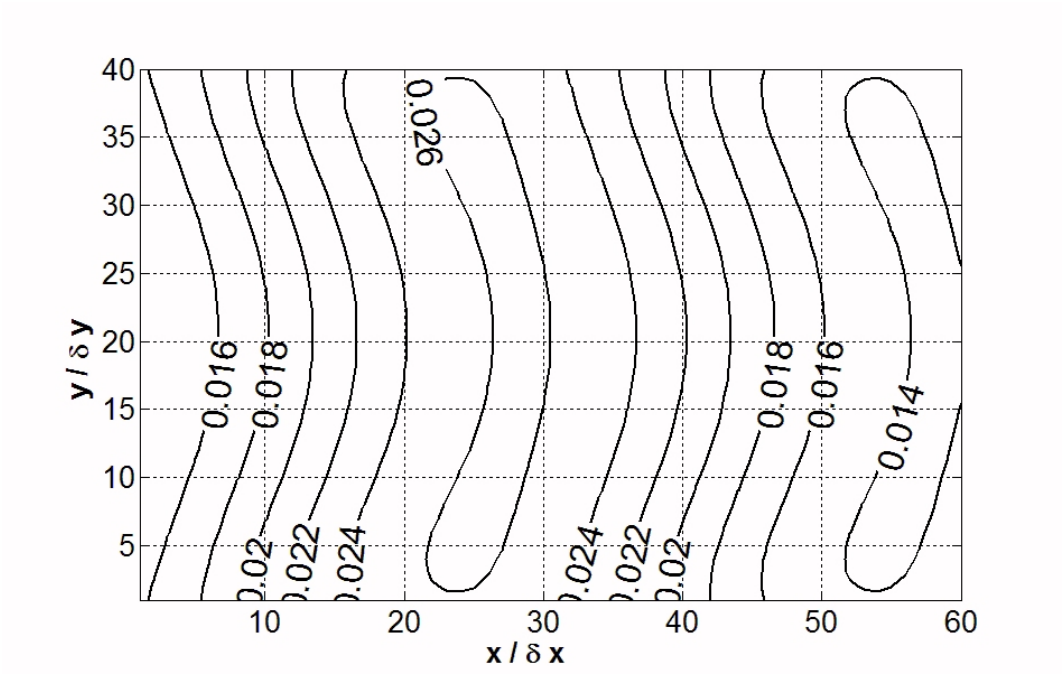

FIG. 1: Iso-contours of the molar concentration y_1 in the domain $[0, L_1] \times [0, L_2]$ at the time step $t = T = 600\,\delta t$, for the solvent test case of a ternary mixture ($y_3 \cong 1$ and consequently $y_1 \cong 0$ and $y_2 \cong 0$).

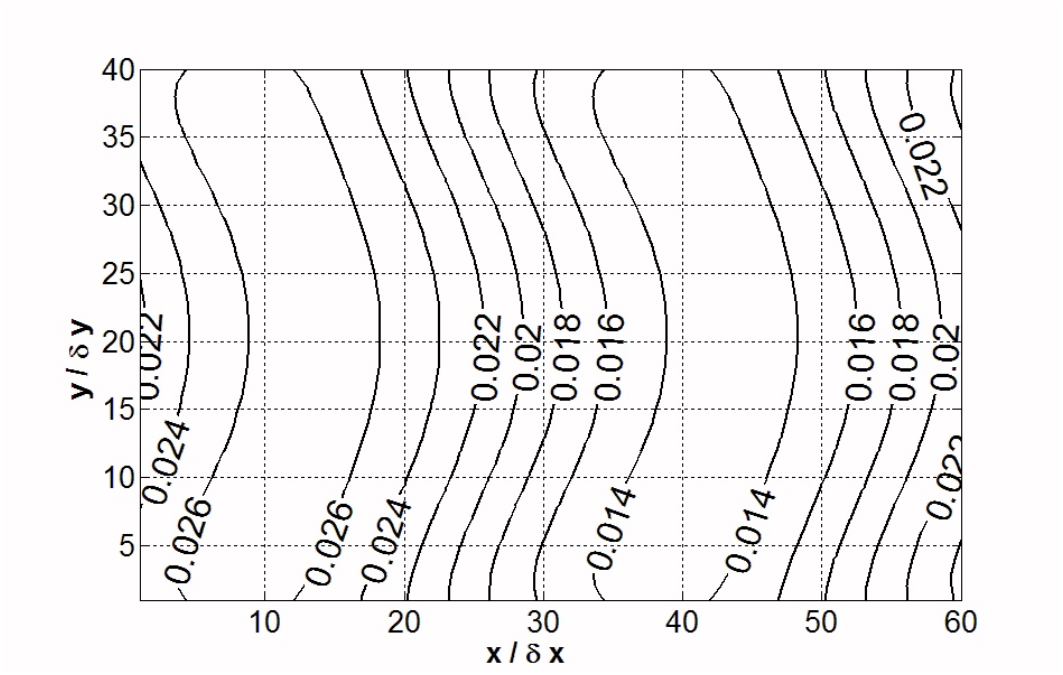

FIG. 2: Iso-contours of the molar concentration y_2 in the domain $[0, L_1] \times [0, L_2]$ at the time step $t = T = 600\,\delta t$, for the solvent test case of a ternary mixture ($y_3 \cong 1$ and consequently $y_1 \cong 0$ and $y_2 \cong 0$).

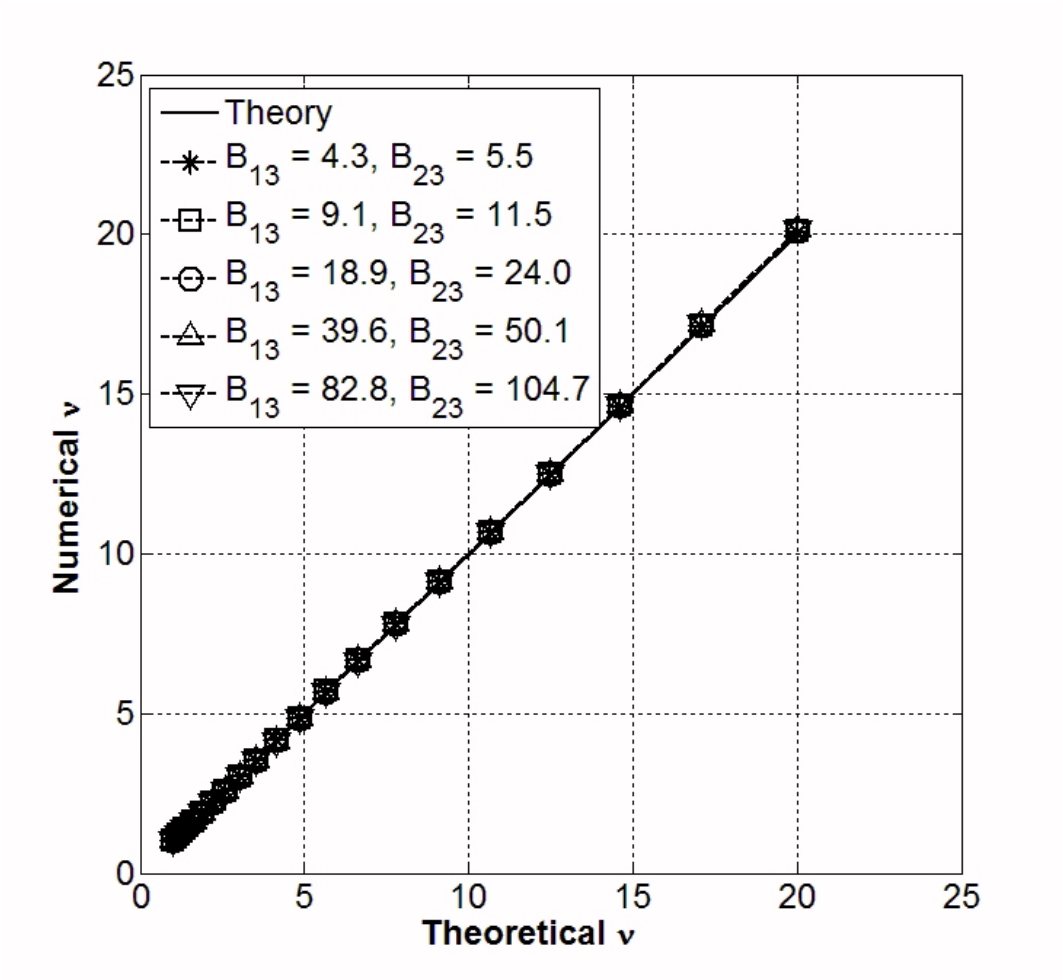

FIG. 3: Solvent test case for a ternary mixture: $y_3 \cong 1$ and consequently $y_1 \cong 0$ and $y_2 \cong 0$. Comparison between theoretical kinematic viscosity $\nu \in [1, 20]$ and the numerical viscosity ν^* of the proposed scheme, measured by Eq. (60), for different values of the Maxwell–Stefan coefficients.

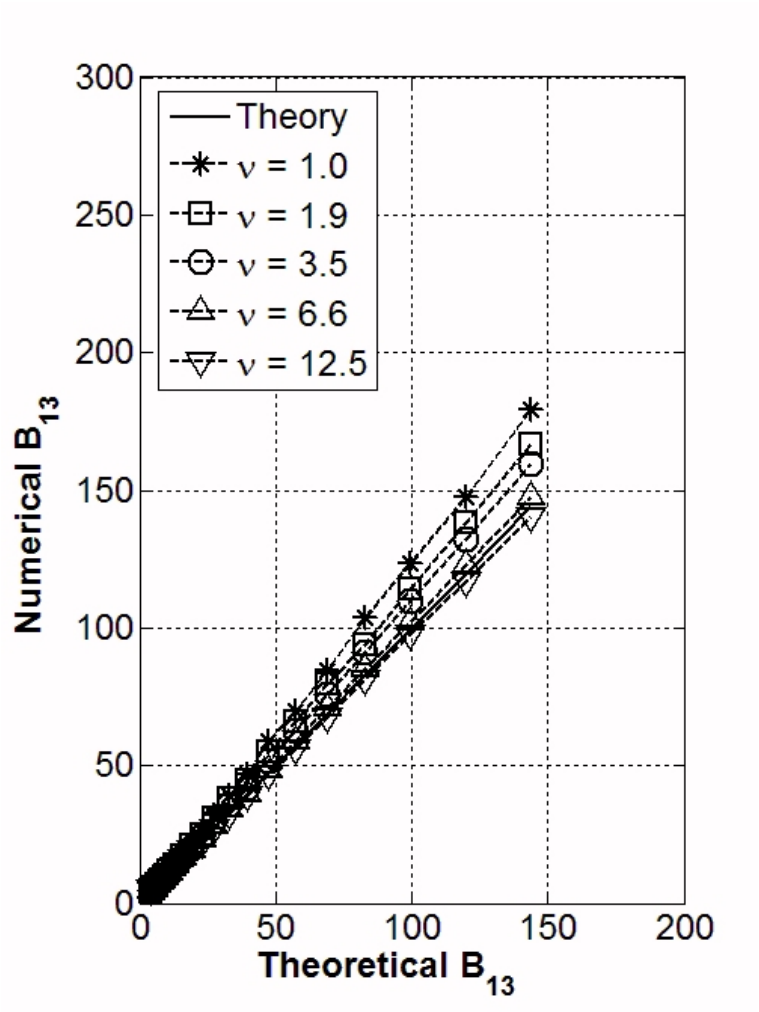

FIG. 4: Solvent test case for a ternary mixture: $y_3 \cong 1$ and consequently $y_1 \cong 0$ and $y_2 \cong 0$. Comparison between theoretical Maxwell–Stefan resistance coefficient for component 1, i.e. B_{13}, with the numerical resistance coefficient B^*_{13} of the proposed scheme, measured by Eq. (64), for different values of the kinematic viscosity.

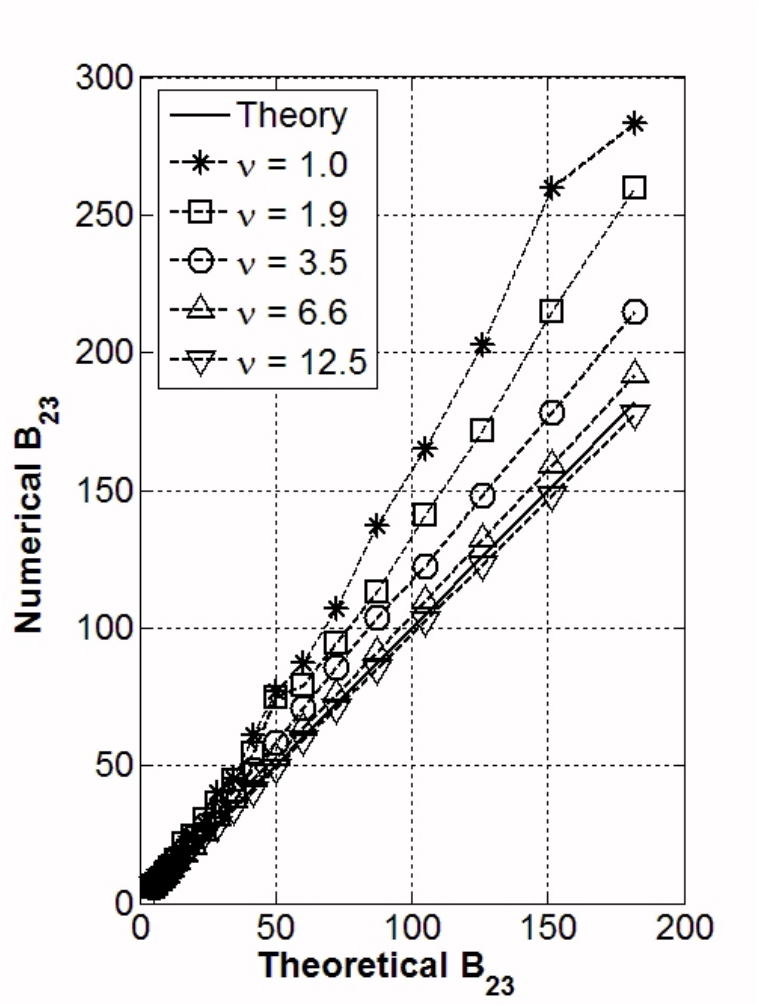

FIG. 5: Solvent test case for a ternary mixture: $y_3 \cong 1$ and consequently $y_1 \cong 0$ and $y_2 \cong 0$. Comparison between theoretical Maxwell–Stefan resistance coefficient for component 2, i.e. B_{23}, with the numerical resistance coefficient B^*_{23} of the proposed scheme, measured by Eq. (65), for different values of the kinematic viscosity.

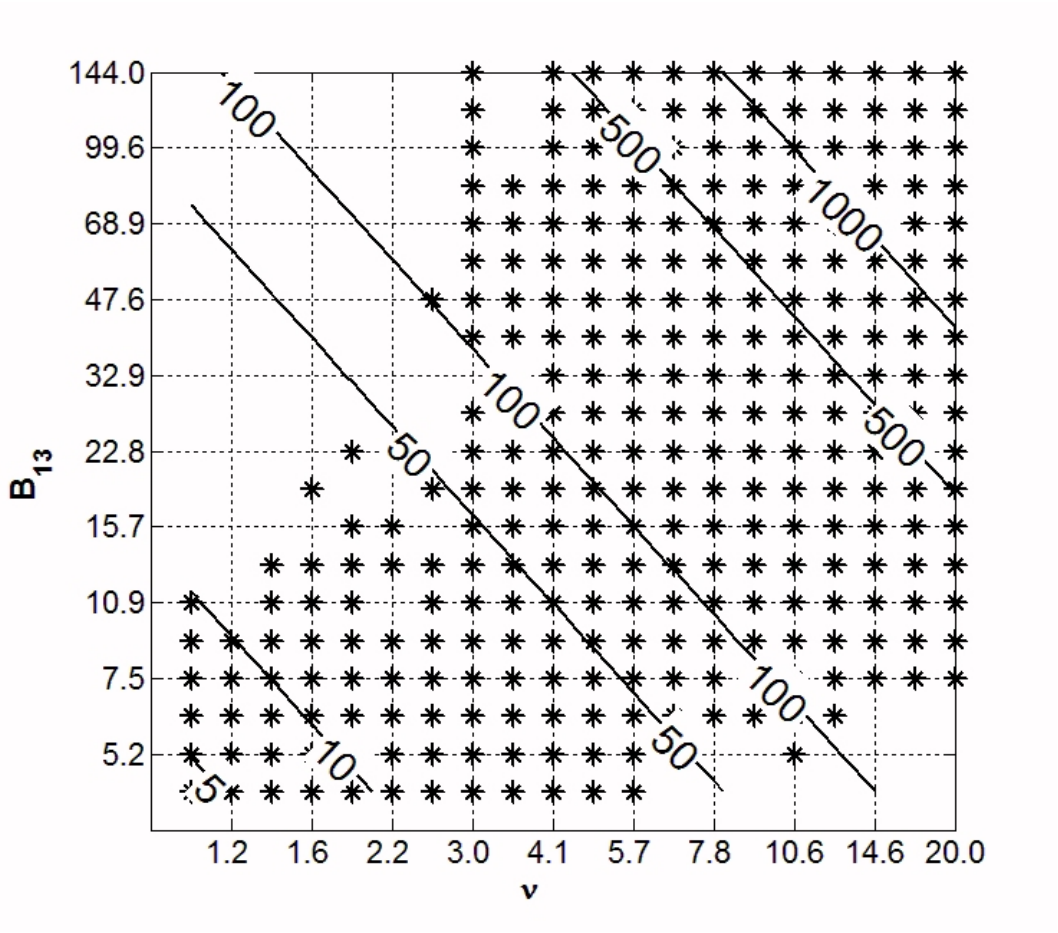

FIG. 6: Solvent test case for a ternary mixture: $y_3 \cong 1$ and consequently $y_1 \cong 0$ and $y_2 \cong 0$. Some simulations ($20 \times 20 = 400$) were performed, for different values of the kinematic viscosity $\nu \in \Gamma_\nu$, where Γ_ν is defined by Eq. (69), and of the Maxwell–Stefan resistance coefficient $B_{13} \in \Gamma_{B13}$, where Γ_{B13} is defined by Eq. (71). The marker '*' means that the numerical error on the measured Schmidt number $\mathsf{Sc}_1^* = \nu^* B_{13}^*$ is acceptable (lower than 10 %). Iso-contours for the Schmidt number Sc_1 are reported too.

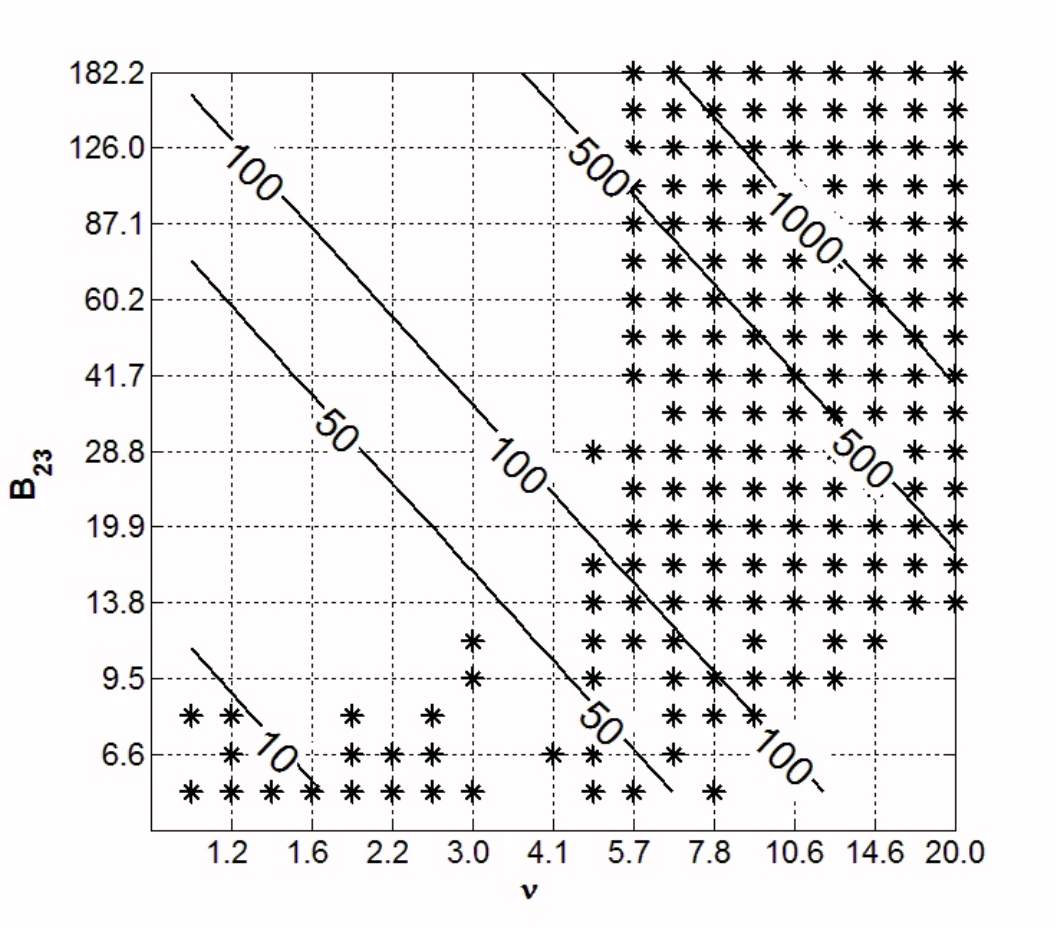

FIG. 7: Solvent test case for a ternary mixture: $y_3 \cong 1$ and consequently $y_1 \cong 0$ and $y_2 \cong 0$. Some simulations ($20 \times 20 = 400$) were performed, for different values of the kinematic viscosity $\nu \in \Gamma_\nu$, where Γ_ν is defined by Eq. (69), and of the Maxwell–Stefan resistance coefficient $B_{23} \in \Gamma_{B23}$, where Γ_{B23} is defined by Eq. (72). The marker '*' means that the numerical error on the measured Schmidt number $\mathsf{Sc}_2^* = \nu^* B_{23}^*$ is acceptable (lower than 10 %). Iso-contours for the Schmidt number Sc_2 are reported too.